Localizing Sources Using a Network of Synchronized Compact Arrays

Ildar R. Urazghildiiev and David E. Hannay

***Abstract*—The problem of passive acoustic estimating the position of a source using a network of synchronized underwater compact arrays is considered. Maximum-likelihood estimators using angle of arrival (AOA), time difference of arrival (TDOA), as well as a combination of AOA/TDOA estimates are developed. The localization accuracy provided by the AOA-based, TDOA-based, and hybrid estimators is evaluated using Cramér–Rao bounds, statistical simulations, and *in situ* test. Test results demonstrated that the efficiency of AOA-based and TDOA-based estimators strongly depends on variances of the AOA and TDOA estimates. Relative efficiency of the hybrid estimator is higher than any of the AOA-based and TDOA-based algorithms.**

***Index Terms*—Compact array, hybrid estimator, maximum-likelihood (ML) estimator, source localization.**

I. Introduction

THE problem of long-term passive acoustic monitoring (PAM) of large ocean areas and localizing vocalizing marine animals, vessels, and other sources is important for many applications. A common approach for solving this problem is based on using large-aperture arrays of fixed synchronized omnidirectional acoustic sensors (hydrophones) [1]–[11]. Positioning through omnidirectional sensors is only based on time difference of arrival (TDOA) of a signal detected on multiple sensors such that PAM systems employing omnidirectional sensors use various TDOA-based localization algorithms. The problem of passive source localization can also be solved using arrays of directional vector sensors [12]–[14]. Although this approach may provide some benefits as compared to omnidirectional sensors, arrays with vector sensors are not considered in this work.

Recent advances in sensor design have resulted in compact arrays of synchronized omnidirectional hydrophones. Such arrays can measure the azimuth and elevation angles of detected signals [15]–[25]. Despite the technical complexity of compact arrays, they are becoming more widespread in underwater PAM. A network of two or more underwater compact arrays can ensure unambiguous localization of surface vessels [15]–[17], [23], marine animals [18]–[22], and other sound producing sources [3], [24] within large marine areas. If compact arrays are asynchronous in the sense that the accurate TDOA of signals detected at different arrays is not possible, only the AOA measurements can be used to estimate the positions of the sources.

The next step forward in PAM system design can be the networks of synchronized compact arrays. In such networks, all sensors used for recording acoustic fields are synchronized. Design and deployment of networks of synchronized compact arrays is an even more complicated technical problem, but such networks can provide several important benefits. One benefit is the ability to combine both TDOA and AOA estimates computed for each detected signal to estimate source position.

The issue of passive multisensor localization of sources using AOA-based, TDOA-based, and hybrid techniques was extensively studied during last decades (see, e.g., [26]–[32] and references therein). The techniques considered in these works were designed mostly for radio signals observed in wireless communication systems and other similar applications. According to these works, both AOA-based and TDOA-based localization techniques require maximization of nonlinear functions such that the main goal of these works was to find certain algebraic solutions to this problem by constructing pseudolinear overdetermined system of equations. The algorithms based on linearizing the equation using Taylor-series expansion [26] and various least squares (LS) techniques [27]–[29], [32] were proposed. These localization algorithms were able to decrease computational complexity, which is important for wireless communication systems. However, for most underwater PAM systems, the basic criterion of efficiency is localization accuracy. This means that accurate rather than fast localization techniques are of higher practical importance.

The TDOA-based localization techniques applicable to underwater PAM systems were studied in many works (see, e.g., [9]–[11], [33]–[35], and references therein). Comparative analysis of several TDOA-based algorithms was performed in [11], and it was reported that the maximum-likelihood (ML) estimator outperformed the hyperbolic fixing and some other suboptimal algorithms. The ML AOA-based localization algorithm applicable to the networks of asynchronous underwater compact arrays was considered in [23]. However, the AOA-based, TDOA-based, and hybrid algorithms applicable to underwater PAM have not been compared in the known literature. It is unclear under which conditions networks of underwater compact arrays can outperform large-aperture arrays of omnidirectional sensors in terms of localization accuracy.

Manuscript received December 7, 2020; accepted May 13, 2021. *(Corresponding author: Ildar R. Urazghildiiev.)*

Associate Editor: B. Thornton

Ildar R. Urazghildiiev is with JASCO Applied Sciences (USA) Inc., Silver Spring, MD 20910 USA (e-mail: ildar.urazghildiiev@jasco.com).

David E. Hannay is with JASCO Applied Sciences (Canada) Ltd., Victoria, BC V8Z 7X8, Canada (e-mail: david.hannay@jasco.com).

Digital Object Identifier 10.1109/JOE.2021.3082758

This study focuses on the problem of estimating the position of a sound source using a network of underwater stationary synchronized compact arrays. The goals of this work are to develop the hybrid ML position estimator combining the AOA and TDOA measurements provided by compact arrays; to derive the closed-form representations for the Cramér–Rao bounds (CRB); and to compare the position estimation accuracy provided by the AOA-based, TDOA-based, and hybrid estimators. The main contribution of this work is the closed-form representations for the hybrid ML estimator, for the CRB, as well as the results of statistical simulations and *in situ* tests comparing the estimation accuracy of three estimators. The intended applications of the proposed technique include, but are not limited to, passive acoustic detection, localization, and tracking of marine animals and vessels, and estimation of population densities and abundances. Section II considers a data model and problem formulation. Section III presents the closed-form representations for the ML estimators. Section IV derives representations for the CRB. Section V presents the results of simulations and *in situ* tests, and Section VI provides discussions and conclusions.

II. Data Model and Problem Formulation

It is assumed that a network of $N \geq 2$ stationary synchronized compact arrays is used to localize a source. Each compact array consists of $M \geq 3$ synchronized sensors (hydrophones) such that a total of NM synchronized sensors are available. The size of arrays specified as the maximum distance between sensors comprising arrays is $d = d_n = \max_{p,q=1\ldots M} \|\boldsymbol{r}_n^p - \boldsymbol{r}_n^q\|$, where $\boldsymbol{r}_n^p$ is the coordinate of the pth sensor of the nth compact array. We assume that the size of arrays is much shorter than the minimum distance between array centers

$$d \ll D = \min_{i \neq j} \|\boldsymbol{r}_i - \boldsymbol{r}_j\| \tag{1}$$

where $\boldsymbol{r}_i = [x_i, y_i]^T \in R^2$ is the position of the center of the ith compact array. For example, two or more compact arrays with the size $d = 1.85$ m placed at the distance $D = 43$ m from each other [23] satisfy this condition. The size d is also much smaller than the maximum possible distance between the source and the centers of the arrays, $d \ll R = \max_{n=1,\ldots,N} \|\boldsymbol{r} - \boldsymbol{r}_n\|$. Under these conditions, sufficiently accurate measurement of the array-to-source distance is not possible for all compact arrays. With $M \geq 3$ sensors not located on a line, each compact array can provide the measurements of two bearings: the azimuth α_n and the elevation angle β_n of the source. However, in many PAM applications, the source depth is not a parameter of interest such that localization is performed in horizontal plane. Beside this, the accuracy of elevation measurements may be insufficient in shallow water due to surface and bottom reflections [17]. Therefore, without loss of generality, only azimuth is considered as the AOA in this work. The array and source positions are represented in a 2-D Cartesian coordinate system with the origin *O*, axis *OX*, and axis *OY* placed on a horizontal surface. The azimuth α_n of a source is defined in a rectangular coordinate system associated with the nth array. It is measured relative to the axis *OY* and obtained by transferring the original coordinate system into the point $\boldsymbol{r}_n$ such that

$$\alpha_n(\boldsymbol{r}) = \tan^{-1} \frac{x - x_n}{y - y_n}. \tag{2}$$

In practice, the positions of compact arrays are measured with some degree of accuracy and may change due to currents and other unpredictable factors. The errors of estimation of the compact array positions may affect the localization accuracy. However, this issue is not considered in this work. We assume that errors in estimating array positions are negligibly small compared to array-to-source distances.

In the general case, multiple moving sources producing various types of sounds, such as vocalizing marine animals and ships, can present within the detection range of compact arrays. The choice of appropriate signal model and corresponding localization technique depends on available data and the goals of investigations. In this work, we assume that signals from different sources do not overlap in time or frequency domain and can be detected separately such that a multisignal situation does not occur. Examples of such signals include impulsive sounds produced by marine animals and ship noise observed in the absence of sounds from other sources.

Prior information about source motion, if available, could potentially be used to enhance source localization. However, the scope of this investigation is limited by localization of sources at the initial stage of spatio-temporal processing when prior information about source motion is not available. We also assume that all motion effects, such as the Doppler shift in the signal frequencies, only affect the AOA and TDOA estimation errors at individual arrays. These effects are not considered here. The position of a source producing the detected signal is described by the vector

$$\boldsymbol{r} = \begin{bmatrix} x \\ y \end{bmatrix} = r \begin{bmatrix} \sin\alpha \\ \cos\alpha \end{bmatrix} \in R^2 \tag{3}$$

where $r = |\boldsymbol{r}\|$ is a distance to the source, symbol $\|\cdot\|$ denotes the vector norm, and α is the source azimuth measured relative to axis *OY*.

For each signal detected by a compact array, its AOA is estimated. In practice, various AOA estimation techniques are applicable to compact arrays. The examples of TDOA-based estimators of azimuths (2) are given in [15]–[20] and [25]. The wideband beamformer and the ML estimators are considered in [36]–[39]. The AOA estimation algorithms used in each individual compact array are not considered in this work. The azimuth estimates obtained by N compact arrays can be represented as

$$\hat{\alpha}_n = \alpha_n(\boldsymbol{r}) + \varepsilon_n, \quad n = 1, \ldots, N \tag{4}$$

where ε_n is the AOA estimation error observed in the nth array.

Because all sensors of the network are synchronized, the TDOA between any ith and jth compact array, i.e., $\hat{\tau}_{i,j}$, can also be measured. In principle, the TDOA estimate can be obtained using any two sensors $\boldsymbol{r}_i^p$ and $\boldsymbol{r}_j^q$ belonging to the ith and jth compact arrays. However, if the assumption (1) holds, TDOA between the array sensors are much smaller than TDOA between the array centers such that TDOA between sensors have very little effect on localization accuracy. Therefore, TDOA estimates

between the centers of compact arrays are used in this work. The TDOA estimates can be represented as

$$\hat{\tau}_{i,j} = \tau_{i,j}\ (\boldsymbol{r}) + \xi_{i,j}, \quad i = 1, \ldots, N-1, \quad j = i+1, \ldots, N \tag{5}$$

where

$$\tau_{i,j}\ (\boldsymbol{r}) = \frac{(\|\boldsymbol{r} - \boldsymbol{r}_i\| - \|\boldsymbol{r} - \boldsymbol{r}_j\|)}{c} \tag{6}$$

is the true TDOA between the centers of the ith and jth compact arrays, $\xi_{i,j}$ is the TDOA estimation error, and c is the speed of sound.

As it was shown in [40], the instances of ambient noise at frequency f are almost uncorrelated at distances $r > (2, \ldots, 3)\lambda$, where $\lambda = c/f$ is the wavelength. This means that if the minimum distance between array centers (1) satisfy the condition

$$D \gg \lambda_{\max} = c/f_{\min} \tag{7}$$

ambient noise observed at the outputs of arrays is uncorrelated. Here, $\lambda_{\max}$ is the maximum wavelength corresponding to the minimum frequency of detected signals, $f_{\min}$. In this case, we can assume that AOA and TDOA estimation errors on array outputs are also uncorrelated, i.e., $E\{\epsilon_i \epsilon_j\} = \sigma_\alpha^2\ \delta_{i,j}$and $E\ \{\xi_k \xi_l\} = \sigma_\tau^2\ \delta_{k,l}$. Here and everywhere, symbol $E\{\cdot\}$ denotes statistical averaging; σ_α^2 and σ_τ^2 are variances of AOA and TDOA estimation errors, respectively; $\delta_{i,j}$ is the Kronecker delta; and ξ_k is the TDOA estimation error ordered in a certain way.

The statistical distributions of AOA and TDOA estimation errors are unknown in practice. They depend on many unpredictable factors, such as the sound propagation environment, the presence of bottom and surface reflections, technical characteristics and deployment of the array, network geometry, the AOA and TDOA estimation algorithms used, signal-to-noise ratio (SNR), and others. Considering the influence of all these factors on the statistical properties of the AOA and TDOA estimation errors and design localization technique minimizing localization error in all possible scenarios is impossible. In this work, we make a standard assumption that the measurement errors ε_n and $\xi_{i,j}$ are independent identically distributed (i.i.d.) Gaussian variables with zero mean and known variances σ_α^2 and σ_τ^2, respectively. This assumption is supported by the central limit theorem stating that when multiple independent random variables are added, their sum tends toward a normal distribution. Thus, the techniques considered in this work are suboptimal unless the measurement errors are normally distributed. The ways of empirical estimating the variances σ_α^2 and σ_τ^2 are considered in Section III.

The efficiency of any estimator can be characterized by the mean square error (MSE) of the estimates $\hat{x}$ and $\hat{y}$ of the source position (3), i.e., $\sigma^2 = E\{(\hat{x} - x)^2 + (\hat{y} - y)^2\}$. Note that MSE coincides with the variance for unbiased estimates. In this article, AOA-based, TDOA-based, and hybrid estimators are compared in terms of relative efficiency specified by the ratio of the MSE they provide. The problems considered here are formulated as follows:

1) to obtain the closed-form representations for the hybrid ML estimator of the vector $\boldsymbol{r}$ (3) using both AOA estimates (4) and TDOA estimates (5);
2) to derive the closed-form representations for the CRB approximating estimation errors;
3) to compare the AOA-based, TDOA-based, and hybrid ML estimators using relative efficiencies σ_A^2/σ_T^2 and $\min\{\sigma_A^2, \sigma_T^2\}/\sigma_H^2$, where σ_A^2, σ_T^2, and σ_H^2 are empirical MSE of the position estimates provided by AOA-based, TDOA-based, and hybrid ML estimators, respectively. The empirical MSE are obtained using statistical simulations and *in situ* test.

III. ML Estimators

Azimuth estimates (4) obtained for a signal detected by N compact arrays can be represented as a random vector

$$\hat{\boldsymbol{\alpha}} = \boldsymbol{\alpha}\,(\boldsymbol{r}) + \boldsymbol{\varepsilon} \in R^N \tag{8}$$

where $\boldsymbol{\alpha}\,(\boldsymbol{r}) = \boldsymbol{\alpha} = [\alpha_1, \ldots, \alpha_N]^T \in R^N$ is the vector of true azimuths and $\boldsymbol{\varepsilon} = [\varepsilon_1, \ldots, \varepsilon_N]^T \in R^N$ is the vector of AOA estimation errors. The mean value and the covariance matrix of vector (8) are

$$E\ \{\hat{\boldsymbol{\alpha}}\} = \boldsymbol{\alpha}, \boldsymbol{C}_{\boldsymbol{\alpha}} = E\left\{(\hat{\boldsymbol{\alpha}} - \boldsymbol{\alpha})\,(\hat{\boldsymbol{\alpha}} - \boldsymbol{\alpha})^T\right\} \in R^{N \times N}. \tag{9}$$

If condition (7) holds, the covariance matrix of vector (8) is diagonal

$$\boldsymbol{C}_{\boldsymbol{\alpha}} = \begin{bmatrix} \sigma_{\alpha 1}^2 & 0 & 0 \\ 0 & \ddots & 0 \\ 0 & 0 & \sigma_{\alpha N}^2 \end{bmatrix} \in R^{N \times N}. \tag{10}$$

where $\sigma_{\alpha n}^2$ is the variance of the AOA estimation errors provided by the nth array. The logarithmic likelihood function of vector $\hat{\boldsymbol{\alpha}}$ is

$$\ln W\ (\hat{\boldsymbol{\alpha}}|\boldsymbol{r}) = k - \frac{1}{2}(\hat{\boldsymbol{\alpha}} - \boldsymbol{\alpha})^T \boldsymbol{C}_\alpha^{-1}\,(\hat{\boldsymbol{\alpha}} - \boldsymbol{\alpha}) \tag{11}$$

where k is a scalar that does not depend on $\boldsymbol{r}$. From (11), the AOA-based ML estimate of vector $\boldsymbol{r}$ is [23]

$$\hat{\boldsymbol{r}}_\alpha = [\hat{x}_\alpha, \hat{y}_\alpha]^T = \arg\max_{x,y} \ln W\,(\hat{\boldsymbol{\alpha}}|\boldsymbol{r})\,. \tag{12}$$

The TDOA estimates (5) of the detected signal can also be presented in vector form as

$$\hat{\boldsymbol{\tau}} = \boldsymbol{\tau}\,(\boldsymbol{r}) + \boldsymbol{\xi} \in R^K \tag{13}$$

where $\boldsymbol{\tau}\,(\boldsymbol{r}) = \boldsymbol{\tau} = [\tau_1, \ldots, \tau_K]^T \in R^K$ is vector consisting of true TDOA estimates, $\tau_{i,j}$, ordered in a certain way; $\boldsymbol{\sigma} = [\xi_1, \ldots, \xi_K]^T \in R^K$ is vector of TDOA estimation errors; and $K = N(N-1)/2$. The mean value and the covariance matrix of vector $\hat{\boldsymbol{\tau}}$ are

$$E\ \{\hat{\boldsymbol{\tau}}\} = \boldsymbol{\tau},\ \boldsymbol{C}_{\boldsymbol{\tau}} = E\left\{(\hat{\boldsymbol{\tau}} - \boldsymbol{\tau})\,(\hat{\boldsymbol{\tau}} - \boldsymbol{\tau})^T\right\} \in R^{K \times K}. \tag{14}$$

If condition (7) holds, the covariance matrix of vector (13) is also diagonal

$$\boldsymbol{C}_{\boldsymbol{\tau}} = \begin{bmatrix} \sigma_{\tau 1}^2 & 0 & 0 \\ 0 & \ddots & 0 \\ 0 & 0 & \sigma_{\tau K}^2 \end{bmatrix} \in R^{K\times K}. \tag{15}$$

The logarithmic likelihood function of vector $\hat{\boldsymbol{\tau}}$ is

$$\ln W\left(\hat{\boldsymbol{\tau}}|\boldsymbol{r}\right) = k - \frac{1}{2}(\hat{\boldsymbol{\tau}} - \boldsymbol{\tau})^T \boldsymbol{C}_{\tau}^{-1}\left(\hat{\boldsymbol{\tau}} - \boldsymbol{\tau}\right). \tag{16}$$

The TDOA-based ML estimate of vector $\boldsymbol{r}$ can be represented as [11]

$$\hat{\boldsymbol{r}}_{\tau} = [\hat{x}_{\tau}, \hat{y}_{\tau}]^T = \arg\max_{x,y} \ln W\left(\hat{\boldsymbol{\tau}}|\boldsymbol{r}\right). \tag{17}$$

Let $\hat{\boldsymbol{\gamma}} = [\hat{\boldsymbol{\alpha}}^T, \hat{\boldsymbol{\tau}}^T]^T \in R^{NK}$ denote the NK-dimensional vector consisting of AOA and TDOA estimates. The logarithmic likelihood function of vector $\hat{\boldsymbol{\gamma}}$ is

$$\ln W\left(\hat{\boldsymbol{\gamma}}|\boldsymbol{r}\right) = k - \frac{1}{2}(\hat{\boldsymbol{\gamma}} - \boldsymbol{\gamma})^T \boldsymbol{C}_{\gamma}^{-1}\left(\hat{\boldsymbol{\gamma}} - \boldsymbol{\gamma}\right). \tag{18}$$

where

$$\boldsymbol{C}_{\gamma} = \begin{bmatrix} \boldsymbol{C}_{\boldsymbol{\alpha}}, \boldsymbol{C}_{\boldsymbol{\alpha\tau}} \\ \boldsymbol{C}_{\boldsymbol{\alpha\tau}}, \boldsymbol{C}_{\boldsymbol{\tau}} \end{bmatrix} \in R^{NK\times NK} \tag{19}$$

is the covariance matrix of $\hat{\boldsymbol{\gamma}}$; and $\boldsymbol{C}_{\boldsymbol{\alpha\tau}} \in R^{N\times K}$ is the matrix specifying correlation between vectors $\hat{\boldsymbol{\alpha}}$ and $\hat{\boldsymbol{\tau}}$. Then, the hybrid ML estimator using both AOA and TDOA measurements provided by the network can be represented as

$$\hat{\boldsymbol{r}}_h = [\hat{x}_h, \hat{y}_h]^T = \arg\max_{x,y} \ln W\left(\hat{\boldsymbol{\gamma}}|\boldsymbol{r}\right). \tag{20}$$

Because AOA and TDOA estimates of the signal are obtained using different algorithms, $\hat{\boldsymbol{\alpha}}$ and $\hat{\boldsymbol{\tau}}$ can be considered as independent random vectors such that $\boldsymbol{C}_{\boldsymbol{\alpha\tau}} = 0$. In this case, the joint likelihood function of vectors $\hat{\boldsymbol{\alpha}}$ and $\hat{\boldsymbol{\tau}}$ can be represented as

$$\ln W\left(\hat{\boldsymbol{\gamma}}|\boldsymbol{r}\right) = \ln W\left(\hat{\boldsymbol{\alpha}}, \hat{\boldsymbol{\tau}}|\boldsymbol{r}\right) = \ln W\left(\hat{\boldsymbol{\alpha}}|\boldsymbol{r}\right) + \ln W\left(\hat{\boldsymbol{\tau}}|\boldsymbol{r}\right). \tag{21}$$

Then, the hybrid ML estimator takes the form

$$\hat{\boldsymbol{r}}_h = [\hat{x}_h, \hat{y}_h]^T = \arg\max_{x,y} \left\{\ln W\left(\hat{\boldsymbol{\alpha}}|\boldsymbol{r}\right) + \ln W\left(\hat{\boldsymbol{\tau}}|\boldsymbol{r}\right)\right\}. \tag{22}$$

If conditions (10) and (15) hold, and all arrays provide the same variances of AOA estimation errors, $\sigma_{\alpha n}^2 = \sigma_{\alpha}^2$, $n = 1, \ldots, N$, and TDOA estimation errors, $\sigma_{\tau k}^2 = \sigma_{\tau}^2$, $k = 1, \ldots, K$, then the joint likelihood function (21) reduces to the following representation:

$$\ln W(\hat{\boldsymbol{\alpha}}, \hat{\boldsymbol{\tau}}|\boldsymbol{r}) = k - \left[\left(2\sigma_{\alpha}^2\right)^{-1} \sum_{n=1}^{N} \left(\hat{\alpha}_n - \alpha_n\right)^2 + \left(2\sigma_{\tau}^2\right)^{-1} \sum_{k=1}^{K} \left(\hat{\tau}_k - \tau_k\right)^2\right]. \tag{23}$$

In this case, the hybrid ML position estimate minimizes the criterion function $\Psi(\hat{\boldsymbol{\alpha}}, \hat{\boldsymbol{\tau}}|\boldsymbol{r})$

$$\hat{\boldsymbol{r}}_h = \arg\min_{x,y} \Psi\left(\hat{\boldsymbol{\alpha}}, \hat{\boldsymbol{\tau}}|\boldsymbol{r}\right) \tag{24}$$

where

$$\Psi\left(\hat{\boldsymbol{\alpha}}, \hat{\boldsymbol{\tau}}|\boldsymbol{r}\right) = \left(2\sigma_{\alpha}^2\right)^{-1} \sum_{n=1}^{N} \left(\hat{\alpha}_n - \alpha_n\right)^2 + \left(2\sigma_{\tau}^2\right)^{-1} \sum_{k=1}^{K} \left(\hat{\tau}_k - \tau_k\right)^2. \tag{25}$$

Representations (22) and (25) show that implementing the hybrid estimator requires knowledge of the variances of AOA and TDOA estimates, σ_{α}^2 and σ_{τ}^2, associated with each detected signal and playing a role of weighting factors. In practice, these variances are unknown and should be replaced by certain estimates computed empirically.

In general, it is difficult to estimate the variance of AOA and TDOA estimates for each detected signal. Therefore, some average values of σ_{α}^2 and σ_{τ}^2 obtained for a set of similar signals can be used in (25). Some estimate of the variance σ_{τ}^2 can also be obtained for each detected signal using available TDOA estimates. Let $\hat{\tau}_{i,j}^{p,q}$ be the TDOA estimate obtained using the pth sensor of the ith array with coordinates $\boldsymbol{r}_i^p$, and the qth sensor of the jth array with coordinates $\boldsymbol{r}_j^q$. If each array has M sensors, then a total of M^2 TDOA estimates can be obtained for each pair of arrays. The estimate of the variance $\sigma_{\tau k}^2$ for the kth pair of arrays is

$$\hat{\sigma}_{\tau k}^2 = M^{-2} \sum_{p} \sum_{q} \left(\hat{\tau}_{i,j}^{p,q} - \bar{\tau}_{i,j}\right)^2 \tag{26}$$

where

$$\bar{\tau}_{i,j} = M^{-2} \sum_{p} \sum_{q} \hat{\tau}_{i,j}^{p,q} \tag{27}$$

is the average TDOA between the ith and jth arrays. The estimates (26) should be substituted in (14) to find the hybrid ML position estimates (22). If all pairs of arrays provide approximately the same variance of TDOA estimates, then (26) can be averaged over all pairs, and the average estimate

$$\hat{\sigma}_{\tau}^2 = K^{-1} \sum_{k=1}^{K} \hat{\sigma}_{\tau k}^2 \tag{28}$$

can be used in (25) to find the hybrid estimates (24).

Note that the TDOA-based 2-D position estimate (17) is unambiguous if the network contains $N \geq 3$ compact arrays. If $N = 2$, the TDOA estimate (5) corresponds to an infinite number of points located on a hyperbola such that $\hat{\boldsymbol{r}}_{\tau}$ becomes unobservable from $\hat{\boldsymbol{\tau}}$. However, the hybrid position estimates (22) and (24) are observable even if $N = 2$. The networks with two separated and synchronized compact arrays are important in practice because they are easier to implement as compared to networks with $N \geq 3$ arrays, but these networks have some specific properties.

Without loss of generality, we can assume that $N = 2$ arrays are placed on the axis *OX*, and the y coordinate of the source is positive, $y > 0$. In this case, the position of a source is at the intersection of two straight lines, $y_{\alpha}^{(n)}(x)$, $n = 1, 2$, which are specified by the equations

$$y_{\alpha}^{(n)}\left(x\right) = k_n \ \left(x - x_n\right) \tag{29}$$

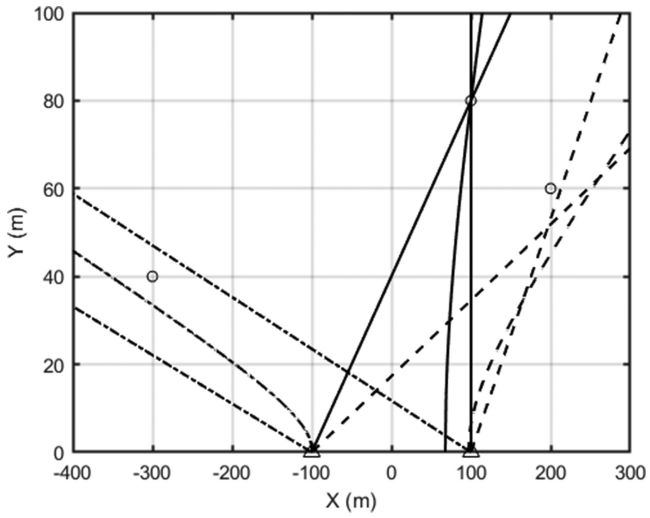

Fig. 1. Functions $\boldsymbol{y}_{\boldsymbol{\alpha}}^{(1)}(\boldsymbol{x})$, $\boldsymbol{y}_{\boldsymbol{\alpha}}^{(2)}(\boldsymbol{x})$, and $\boldsymbol{y}_{\boldsymbol{\tau}}(\boldsymbol{x})$ computed for the actual AOA and TDOA values (solid lines), small AOA and TDOA measurement errors (dashed lines), and large errors (dash-dotted lines). The symbols "○" show the source positions, and the symbols "Δ" display the positions of the arrays.

where $k_n = \cos\alpha_n / \sin\alpha_n$ is the coefficient determining the slope of the nth line, and x_n is the x coordinate of the nth array.

The ML AOA estimate (12) can be found directly from (29) by substituting the AOA estimates (8) in (29)

$$\hat{x}_\alpha = \frac{\hat{k}_1 x_1 - \hat{k}_2 x_2}{\hat{k}_1 - \hat{k}_2}\ ,\ \ \hat{y}_\alpha = \hat{k}_1(\hat{x}_\alpha - x_1) = \hat{k}_2\,(\hat{x}_\alpha - x_2) \tag{30}$$

where $\hat{k}_n = \cos\hat{\alpha}_n / \sin\hat{\alpha}_n$.

The infinity set of TDOA-based ML position estimates (17) is specified by the hyperbolae

$$y_\tau\,(x) = \frac{b\sqrt{x^2 - a^2}}{a} \tag{31}$$

where $a = \hat{\tau}c$; $\hat{\tau}$ is the TDOA estimate (13); $b = \sqrt{(D/2)^2 - (a/2)^2}$; D is the distance between two arrays; and c is the speed of sound. The hyperbolae (31) has an asymptote with the slope

$$\alpha_\tau = \tan^{-1}\frac{b}{a}.$$

If $x_1 < x_2$ and $y > 0$, then the following condition holds for the azimuths:

$$\alpha_1 > \alpha_\tau > \alpha_2. \tag{32}$$

If AOA and TDOA estimates are free from errors, i.e., $\hat{\tau} = \tau$ and $\hat{\alpha}_{1,2} = \alpha_{1,2}$, then $y_\alpha^{(1)}(x)$, $y_\alpha^{(2)}(x)$, and $y_\tau(x)$ intersect in a source position $\boldsymbol{r}$ (see Fig. 1, solid lines). In the presence of AOA and TDOA measurement errors, various situations may occur. If the measurement errors are small and condition (32) holds for the azimuth estimates, $\hat{\alpha}_1 > \hat{\alpha}_\tau > \hat{\alpha}_2$, the straight lines $y_\alpha^{(1)}(x)$ and $y_\alpha^{(2)}$ and the hyperbolae $y_\tau(x)$ intersect near the source positions (see Fig. 1, dashed lines). In this case, the maximum of the criterion function $\Psi(\hat{\boldsymbol{\alpha}}, \hat{\boldsymbol{\tau}}|\boldsymbol{r})$ exists and the hybrid estimator (25) produces regular localization error. If condition (32) does not hold because $\hat{\alpha}_1 \le \hat{\alpha}_2$, $\hat{\alpha}_\tau < \hat{\alpha}_2$, or $\hat{\alpha}_\tau > \hat{\alpha}_1$, then the straight lines $y_\alpha^{(1)}(x)$ and $y_\alpha^{(2)}$ do not intersect for $y > 0$ (see Fig. 1, dash-dotted lines). In this situation, the maximum of $\Psi(\hat{\boldsymbol{\alpha}}, \hat{\tau}|\boldsymbol{r})$ either does not exist or is located at a very long distance from the source, and the hybrid estimator (25) produces abnormal error (outlier). As a result, in the case $N = 2$ arrays, both the AOA-based and hybrid estimators should also be characterized by the probability of occurring outliers. The AOA-based and hybrid estimates should be accepted if condition (32) holds and rejected otherwise.

IV. Cramér–Rao Bounds (CRB)

The CRB specify the lowest variance that any unbiased linear estimator can achieve [38], [41]. We derive the closed-form representations specifying the CRB of the ML hybrid position estimate (24) under the assumption of uncorrelated vectors $\hat{\boldsymbol{\alpha}}$ and $\hat{\boldsymbol{\tau}}$.

The CRB of the hybrid estimates of 2-D vector $\boldsymbol{r}$ (3) can be represented in the form [37], [38], [41]

$$\mathrm{CRB}\,(\boldsymbol{r}) = \boldsymbol{F}(\boldsymbol{r})^{-1} = \begin{bmatrix} \mathrm{CRB}_h^{xx} & \mathrm{CRB}_h^{xy} \\ \mathrm{CRB}_h^{yx} & \mathrm{CRB}_h^{yy} \end{bmatrix} \in R^{2\times 2} \tag{33}$$

where

$$\begin{aligned} \boldsymbol{F}\,(\boldsymbol{r}) &= E\left[\left(\frac{\partial \ln W\,(\hat{\boldsymbol{\alpha}}, \hat{\boldsymbol{\tau}}|\boldsymbol{r})}{\partial \boldsymbol{r}}\right)^T \left(\frac{\partial \ln W\,(\hat{\boldsymbol{\alpha}}, \hat{\boldsymbol{\tau}}|\boldsymbol{r})}{\partial \boldsymbol{r}}\right)\right] \\ &= -E\left[\frac{\partial^2 \ln W\,(\hat{\boldsymbol{\alpha}}, \hat{\boldsymbol{\tau}}|\boldsymbol{r})}{\partial \boldsymbol{r}\partial \boldsymbol{r}^{\boldsymbol{T}}}\right] \in R^{2\times 2} \end{aligned} \tag{34}$$

is the Fisher information matrix (FIM). Taking into account (21), the FIM can be represented as a sum of two terms

$$\boldsymbol{F}\,(\boldsymbol{r}) = \boldsymbol{F}_\alpha\,(\boldsymbol{r}) + \boldsymbol{F}_\tau\,(\boldsymbol{r}) \tag{35}$$

where

$$\boldsymbol{F}_\alpha\,(\boldsymbol{r}) = \begin{bmatrix} F_\alpha^{xx} & F_\alpha^{xy} \\ F_\alpha^{yx} & F_\alpha^{yy} \end{bmatrix} \text{ and } \boldsymbol{F}_\tau\,(\boldsymbol{r}) = \begin{bmatrix} F_\tau^{xx} & F_\tau^{xy} \\ F_\tau^{yx} & F_\tau^{yy} \end{bmatrix} \tag{36}$$

are FIMs corresponding to AOA-based (11) and TDOA-based (16) likelihood functions, respectively. Performing statistical averaging of the likelihood function (11), the elements of FIM $\boldsymbol{F}_\alpha(\boldsymbol{r})$ can be represented as

$$\begin{aligned} F_\alpha^{xx} &= \nabla_\alpha^{xT}\,\boldsymbol{C}_\alpha^{-1}\nabla_\alpha^x \\ F_\alpha^{xy} &= F_\alpha^{yx} = \nabla_\alpha^{xT}\,\boldsymbol{C}_\alpha^{-1}\nabla_\alpha^y \\ F_\alpha^{yy} &= \nabla_\alpha^{yT}\,\boldsymbol{C}_\alpha^{-1}\nabla_\alpha^y \end{aligned} \tag{37}$$

where

$$\nabla_\alpha^x = \frac{\partial \boldsymbol{\alpha}\,(\boldsymbol{r})}{\partial x} \in R^N,\quad \nabla_\alpha^y = \frac{\partial \boldsymbol{\alpha}\,(\boldsymbol{r})}{\partial y} \in R^N \tag{38}$$

are vectors of partial derivatives of the azimuths over the coordinates x and y, respectively. Partial derivatives of the azimuths (38) are

$$\frac{\partial \alpha_n}{\partial x} = \frac{y - y_n}{d_n^2} \tag{39a}$$

$$\frac{\partial \alpha_n}{\partial y} = -\frac{x - x_n}{d_n^2} \tag{39b}$$

where $d_n^2 = (x - x_n)^2 + (y - y_n)^2$. Partial derivatives (38) in polar coordinates are given in [23].

The elements of FIM $\boldsymbol{F}_\tau(\boldsymbol{r})$ can be obtained by performing statistical averaging of the likelihood function (16)

$$\begin{aligned} F_\tau^{xx} &= \nabla_\tau^{xT}\, \boldsymbol{C}_\tau^{-1} \nabla_\tau^x \\ F_\tau^{xy} &= F_\tau^{yx} = \nabla_\tau^{xT}\, \boldsymbol{C}_\tau^{-1} \nabla_\tau^y \\ F_\tau^{yy} &= \nabla_\tau^{yT}\, \boldsymbol{C}_\tau^{-1} \nabla_\tau^y \end{aligned} \tag{40}$$

where

$$\begin{aligned} \nabla_\tau^x &= \frac{\partial \boldsymbol{\tau}\,(\boldsymbol{r})}{\partial x} \in R^K \\ \nabla_\tau^y &= \frac{\partial \boldsymbol{\tau}\,(\boldsymbol{r})}{\partial y} \in R^K \end{aligned} \tag{41}$$

are vectors of partial derivatives of TDOAs over the coordinates x and y, respectively. Partial derivatives of TDOA $\tau_{i,j}(\boldsymbol{r})$ are

$$\frac{\partial \tau_{i,j}\,(\boldsymbol{r})}{\partial x} = \frac{1}{c}\left(\frac{x - x_i}{\|\boldsymbol{r} - \boldsymbol{r}_i\|} - \frac{x - x_j}{\|\boldsymbol{r} - \boldsymbol{r}_j\|}\right) \tag{42a}$$

$$\frac{\partial \tau_{i,j}\,(\boldsymbol{r})}{\partial y} = \frac{1}{c}\left(\frac{y - y_i}{\|\boldsymbol{r} - \boldsymbol{r}_i\|} - \frac{y - y_j}{\|\boldsymbol{r} - \boldsymbol{r}_j\|}\right). \tag{42b}$$

Substituting (37)–(42) in (35) gives closed-form representations for the FIM $\boldsymbol{F}(\boldsymbol{r})$. Corresponding representation in polar coordinates can be obtained similarly by computing partial derivatives (39) and (42) over the parameters $\{r, \alpha\}$.

If the hybrid position estimates are unbiased, the lower bound on their variance and MSE is

$$\sigma_H^2 = E\left\{(\hat{x}_h - x)^2 + (\hat{y}_h - y)^2\right\} \geq \mathrm{CRB}_h \tag{43}$$

where $\mathrm{CRB}_h = \mathrm{CRB}_h^{xx} + \mathrm{CRB}_h^{yy}$. Because the FIMs $\boldsymbol{F}_\alpha(\boldsymbol{r})$ and $\boldsymbol{F}_\tau(\boldsymbol{r})$ are positive definite, determinant of $\boldsymbol{F}(\boldsymbol{r})$ has the property

$$\det(\boldsymbol{F}(\boldsymbol{r})) \geq \det(\boldsymbol{F}_\alpha(\boldsymbol{r})) + \det(\boldsymbol{F}_\tau(\boldsymbol{r})).$$

Hence

$$\begin{aligned} &\det\left(\mathrm{CRB}(\boldsymbol{r})\right) \\ &= \det(\boldsymbol{F}(\boldsymbol{r}))^{-1} \leq \left(\det(\boldsymbol{F}_\alpha(\boldsymbol{r})) + \det(\boldsymbol{F}_\tau(\boldsymbol{r}))\right)^{-1} \end{aligned}$$

and the following property holds:

$$\mathrm{CRB}_h \leq \min\left[\mathrm{CRB}_\alpha,\ \mathrm{CRB}_\tau\right] \tag{44}$$

where $\mathrm{CRB}_\alpha = \mathrm{CRB}_\alpha^{xx} + \mathrm{CRB}_\alpha^{yy}$ and $\mathrm{CRB}_\tau = \mathrm{CRB}_\tau^{xx} + \mathrm{CRB}_\tau^{yy}$. This property implies that CRB of the hybrid ML estimator (22) is not higher than the CRB provided by any of the AOA-based (12) or TDOA-based (17) estimators separately, and relative efficiency in terms of CRB is

$$\frac{\min\left[\mathrm{CRB}_\alpha,\ \mathrm{CRB}_\tau\right]}{\mathrm{CRB}_h} \geq 1. \tag{45}$$

Because the FIMs $\boldsymbol{F}_\alpha(\boldsymbol{r})$ and $\boldsymbol{F}_\tau(\boldsymbol{r})$ depend on the covariance matrices $\boldsymbol{C}_\alpha$and $\boldsymbol{C}_\tau$, relative efficiency of the AOA-based and TDOA-based estimators can be any positive value, $0 < \mathrm{CRB}_\alpha/\mathrm{CRB}_\tau < \infty$. In practice, this means that either an AOA-based or TDOA-based estimator can potentially be more efficient depending on the variances of AOA and TDOA estimation errors, σ_α^2 and σ_τ^2, observed in a given situation.

For the special case of $N = 2$ arrays, the FIM $\boldsymbol{F}_\tau(\boldsymbol{r})$ is singular and the CRB_τ for the TDOA-based estimates does not exist. However, FIM $\boldsymbol{F}_\alpha(\boldsymbol{r})$ for the AOA-based estimates is nonsingular such that and $\boldsymbol{F}(\boldsymbol{r})$ (35) is also nonsingular and $\mathrm{CRB}(\boldsymbol{r})$ for the hybrid estimator can be computed. Because determinant of $\boldsymbol{F}(\boldsymbol{r})$ has the property $\det(\boldsymbol{F}(\boldsymbol{r})) \geq \det(\boldsymbol{F}_\alpha(\boldsymbol{r}))$, CRB of AOA-based and hybrid estimates satisfies the condition

$$\mathrm{CRB}_h \leq \mathrm{CRB}_\alpha. \tag{46}$$

From (46), it follows that CRB of the hybrid ML estimator (22) is not higher than the CRB provided by the AOA based (12) estimator, and its relative efficiency in terms of CRB is

$$\frac{\mathrm{CRB}_\alpha}{\mathrm{CRB}_h} \geq 1. \tag{47}$$

Representations (45) and (47) show that the relative potential efficiency of the hybrid ML estimator is not lower than any of the AOA-based and TDOA-based estimators.

V. Test Results

The main goal of the tests was to evaluate localization accuracy and relative efficiency of the AOA-based, TDOA-based, and the hybrid estimators using empirical MSE of the position estimates, σ_A^2, σ_T^2, and σ_H^2, provided by these estimators. Because data recordings required for comprehensive *in situ* tests using $N > 2$ arrays were unavailable in this work, the localization accuracy was tested using statistical simulations. For the case of $N = 2$ arrays, we performed simulations and *in situ* tests using data collected by an advanced underwater listening station (ULS) designed by JASCO Applied Sciences (Canada) in collaboration with Vancouver Fraser Port Authority's Enhancing Cetacean Habitat Observation Program and Transport Canada. The ULS consists of two synchronized compact tetrahedral arrays of $M = 4$ hydrophones each.

A. Statistical simulations

Simulations were conducted for a hypothetical network consisting of $N = 3$ and for ULS with $N = 2$ synchronized compact arrays of underwater recorders. We assumed that each compact array consisted of $M \geq 3$ hydrophones spaced in the configuration that provide unambiguous estimation of azimuths (4) using broadband BF-based estimator [39] or similar algorithms. The arrays were uniformly spaced on a circle with 302-m radius. The coordinates of the arrays were $\boldsymbol{r}_1 = [-130.7,\ 75.5]^T$, $\boldsymbol{r}_2 = [130.7,\ 75.5]^T$, and $\boldsymbol{r}_3 = [0,\ -151.0]^T$ m for the network consisting of $N = 3$ arrays, and $\boldsymbol{r}_1 = [-151.0,\ 0.0]^T$ and $\boldsymbol{r}_2 = [151.0,\ 0.0]^T$ m for the ULS, respectively. The array positions are shown in Fig. 2.

Statistical simulations were conducted for ten positions simulating the locations of a source. Simulation points had horizontal ranges $r = \sqrt{x^2 + y^2} = [100,\ 200, \ldots, 1000]$ m from the origin, and the azimuth $\alpha = 70^\circ$. The maximum range was

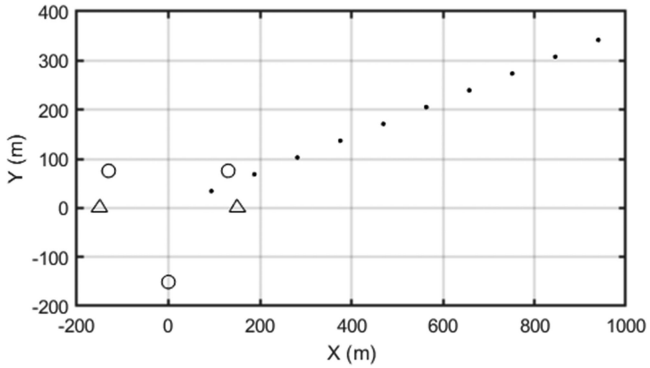

Fig. 2. Locations of compact arrays from the hypothetical network (symbol "○") and from the ULS (symbol "Δ"). The simulated source positions are shown by dots.

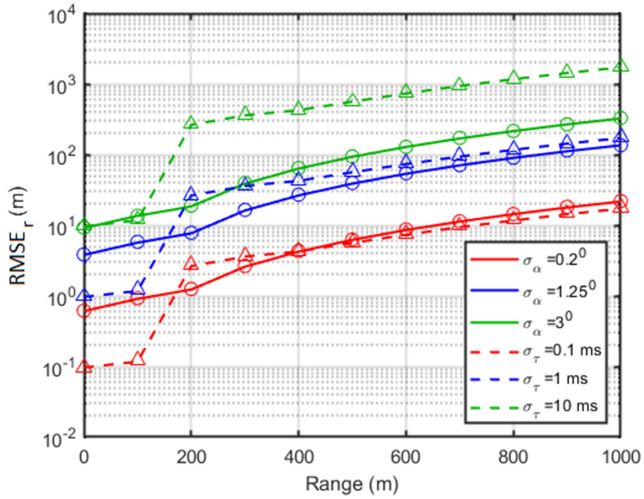

Fig. 3. Network with $\boldsymbol{N} = 3$ arrays: RMSE of position estimates provided by the AOA-based (symbol "○") and TDOA-based (symbol "Δ") estimators as functions of AOA estimation errors, $\boldsymbol{\sigma_\alpha}$, TDOA estimation errors, $\boldsymbol{\sigma_\tau}$, and horizontal range, $\boldsymbol{r}$. Solid lines show the square root of the CRB for the AOA-based estimator, $\sqrt{\mathrm{CRB}_{\boldsymbol{\alpha}}}$. Dashed lines display the square root of the CRB for the TDOA-based estimator, $\sqrt{\mathrm{CRB}_{\boldsymbol{\tau}}}$.

taken to provide sufficiently high detection probability of sounds with the source level from 146 to 190 dB re 1 μPa^2 typical for low- and midfrequency sounds produced by marine mammals [42]–[45]. The simulated source positions are shown in Fig. 2. For each position, the empirical root mean square error (RMSE)

$$\mathrm{RMSE} = \hat{\sigma} = \sqrt{(L)^{-1}\sum_{l=1}^{L}\Delta_l^2} \tag{48}$$

was computed using $L = 1000$ runs. Here, $\Delta_l^2 = (\hat{x}_l - x)^2 + (\hat{y}_l - y)^2$, and $\hat{x}_l$ and $\hat{y}_l$ are the AOA-based (12), TDOA-based (17), or hybrid (24) position estimates obtained in the lth simulation run, respectively. In each run, AOA and TDOA estimation errors were simulated as random i.i.d. Gaussian variables with zero mean and various standard deviations (STD) of AOA estimation errors, σ_α, and TDOA estimation errors, σ_τ.

In practice, the parameters σ_α and σ_τ both depend on many factors, such as sample rate, signal center frequency, bandwidth, SNR, array geometry, and various effects of sound propagation in the water. Considering all these factors were outside the scope of this work. However, to make the simulation results realistic, the empirical variances of azimuth and TDOA estimation errors were taken from test results presented in the literature.

The research work in [39] reported the STD of azimuth measurements, σ_α, varied from 0.2° to 3° depending on signal bandwidth, minimum frequency, and SNR. These values were obtained for beluga whale (*Delphinapterus leucas*) vocalizations with >22 ms duration; 0,…,3000 Hz minimum frequency; 25,…,500 Hz bandwidth; and 10,…,35 dB SNR. The STD of TDOA measurements, σ_τ, are obtained for linear frequency modulated signals at frequency from 200 to 1000 Hz and the SNR higher than 10 dB, varied from 1 to 100 ms [11]. Based on the results of these works, the parameters $\sigma_\alpha = [0.2^\circ, 1.25^\circ, 3.0^\circ]$ and $\sigma_\tau = [0.1;\ 1; 10]$ ms were used for simulations.

The first goal of the statistical simulations was to evaluate and compare the RMSE (48) provided by the AOA-based (12) and TDOA-based (17) estimators for the case of $N = 3$ arrays. The simulation scenario evaluated the dependence of the RMSE on the horizontal range r. The simulation results as well as the corresponding CRB obtained for the network with $N = 3$ arrays are shown in Fig. 3. For this simulation scenario, the relative empirical efficiency of the AOA and TDOA-based estimators was

$$\frac{\sigma_A^2}{\sigma_T^2} = 0.005 \ldots 59.$$

The second goal was to evaluate the impact of the AOA estimation errors, σ_α , and TDOA estimation errors, σ_τ, on the position estimation accuracy provided by the hybrid ML estimator (24). For this purpose, RMSE (48) of the hybrid estimator was computed for all simulated source positions. In this test, we also compared CRB of the AOA-based, TDOA-based, and hybrid estimators. In all scenarios, the inequalities (44) and (45) was true. The results of simulation and the corresponding CRB obtained for the farthest simulated position located at the range $r = 1000$ m from the center of the network are shown in Fig. 4.

Relative empirical efficiency of the hybrid estimator computed for all simulated positions and all values of σ_α and σ_τ was $\min\{\sigma_A^2, \sigma_T^2\}/\sigma_H^2 = 1.001 \ldots 8.56$, which complies with (45).

For the case of $\boldsymbol{N} = 2$ arrays, the TDOA-based estimator is inapplicable such that we compared the AOA-based (30) and the hybrid (24) estimators only. As it was mention in Section III, for two-array networks, there exists a nonzero probability of outliers in position estimates occurring if condition (32) for azimuth estimates does not hold. Comprehensive study of the statistical properties of outliers was outside the scope of this work. The probability of outliers as function of $\boldsymbol{\sigma_\alpha}$ and $\boldsymbol{\sigma_\tau}$ was evaluated for all simulation points. It was found that the probability of outliers increases as AOA estimation errors, TDOA estimation errors, and distance to the source increase (see also Fig. 1). The highest probability of outliers was observed for the farthest

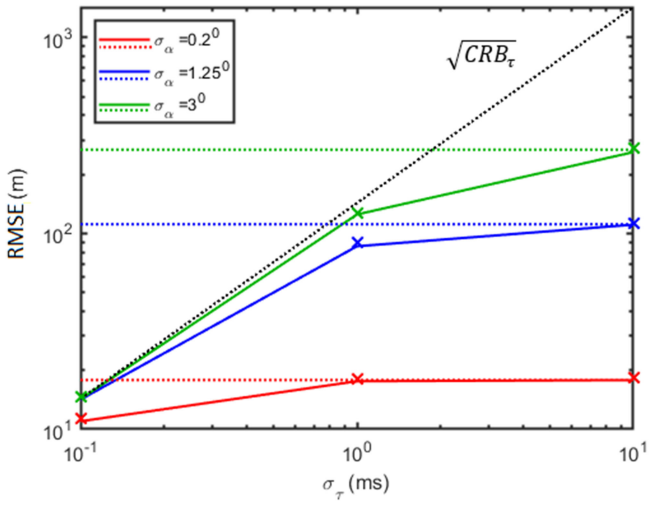

Fig. 4. Network with $\boldsymbol{N} = 3$ arrays: RMSE of position estimates provided by the hybrid estimator (symbol "×") as functions of AOA estimation errors, $\boldsymbol{\sigma_\alpha}$, and TDOA estimation errors, $\boldsymbol{\sigma_\tau}$. The square root of the CRB (43) for the hybrid estimator (44), $\sqrt{\text{CRB}_{\boldsymbol{h}}}$, are shown by the solid lines. Dashed lines display the values of $\sqrt{\text{CRB}_{\boldsymbol{\alpha}}}$ (colored lines) and $\sqrt{\text{CRB}_{\boldsymbol{\tau}}}$ (black line) for the AOA-based estimates and TDOA-based ML estimates, respectively.

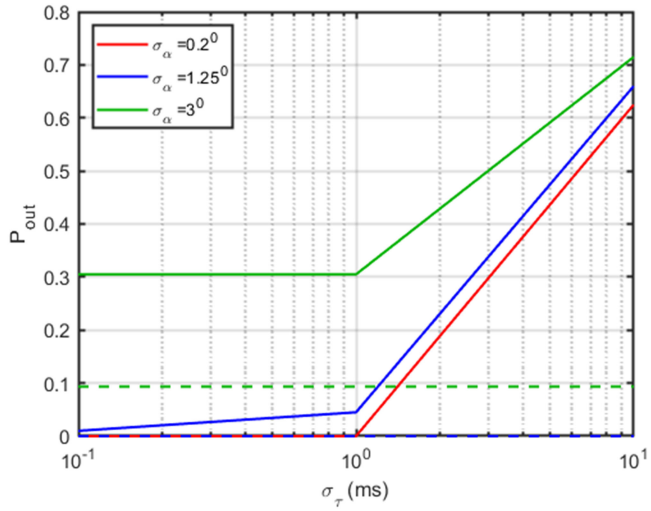

Fig. 5. Network with $\boldsymbol{N} = 2$ arrays: The probability of outliers provided by the AOA-based estimator (dashed lines) and hybrid estimator (solid lines) as functions of AOA estimation errors, $\boldsymbol{\sigma_\alpha}$, and TDOA estimation errors, $\boldsymbol{\sigma_\tau}$.

simulated position ($\boldsymbol{r} = 1000$ m). The empirical probabilities of outliers obtained for this position are represented in Fig. 5.

The empirical RMSE of position estimates (48) was computed after removing outliers such that only estimates with regular errors obtained when condition (32) satisfied were used. The RMSE provided by the AOA-based and hybrid estimators as functions of the horizontal range, r, AOA estimation errors, σ_α, and TDOA estimation errors, σ_τ, are shown in Fig. 6. The corresponding CRB values are also shown in this figure. Relative empirical efficiency of the AOA and hybrid estimators was $\sigma_A^2/\sigma_H^2 = 1.05 \ldots 10.2$.

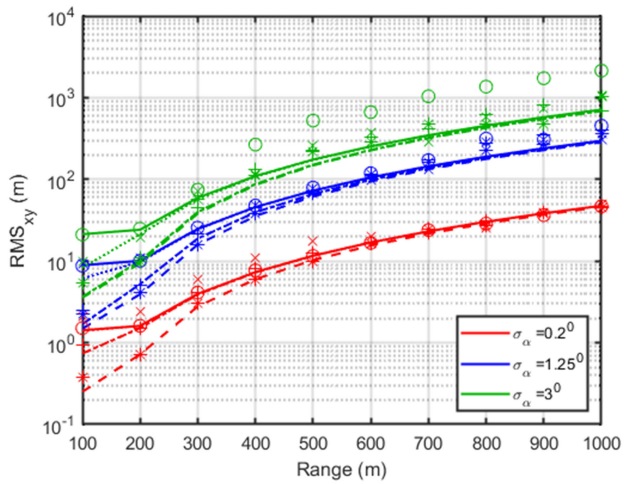

Fig. 6. Network with $\boldsymbol{N} = 2$ arrays: RMSE of position estimates as functions of AOA estimation errors, $\boldsymbol{\sigma_\alpha}$, TDOA estimation errors, $\boldsymbol{\sigma_\tau}$, and horizontal range, $\boldsymbol{r}$. The AOA-based estimator is represented by symbol "∘", and the hybrid estimator is shown by symbols "∗" ($\boldsymbol{\sigma_\tau} = 0.1$ ms), symbols "+" ($\boldsymbol{\sigma_\tau} = 1$ ms), and "×" ($\boldsymbol{\sigma_\tau} = 10$ ms). Solid lines show the square root of the CRB for the AOA-based estimator, $\sqrt{\text{CRB}_{\boldsymbol{\alpha}}}$. Dashed, dash-dotted and dotted lines represent the square root of the CRB for the hybrid estimator, $\sqrt{\text{CRB}_{\boldsymbol{h}}}$, corresponding to the STD $\boldsymbol{\sigma_\tau} = 0.1$, 1, and 10 ms, respectively.

B. *In Situ Test*

The ULS designed by JASCO Applied Sciences (Canada) was used as a network with $N = 2$ arrays for *in situ* testing. The ULS was deployed in Boundary Pass, BC, Canada, between the in- and outbound shipping lanes that lead to and from Vancouver ports. Since June 10, 2020, the ULS has been performing real-time measurements of underwater noise emissions of vessels passing through Boundary Pass. Each array consisted of $M = 4$ GeoSpectrum M-36 hydrophones located in tetrahedral configuration and sampled at 512 kHz using the eight-channel analog-to-digital converter to ensure simultaneous sampling of all eight hydrophones. Combined hydrophone sensitivity and current-to-voltage converter board sensitivity were -165 dB re 1 V/μPa at 250 Hz. The hydrophones were spaced at $d = 1.65$ m distance, which provided the half-wavelength frequency of the arrays $f_{\lambda/2} \approx 440$ Hz. The arrays were deployed at the ocean bottom at a 192-m depth. The array positions and orientations were measured during the deployment and calibrated using a transponder with known coordinates [17], [24]. The array positions were represented in a 2-D Cartesian coordinate system with the origin O, located between the centers of array, and the axis OX placed in a horizontal surface along a line connecting array centers. Locations of the centers of ULS compact arrays are shown in Fig. 7.

The goals of *in situ* testing were to evaluate AOA and TDOA estimation errors provided by the ULS and the relative efficiency of AOA-based and hybrid localization algorithms. For this purpose, we used $K = 6$ passes of ships with known automatic identification system (AIS)-based coordinates. The AIS tracks were interpolated and corrected for timing errors and systematic offsets using azimuth and elevation estimates of the dominant noise source (propeller) of the ships. The corrected trajectories

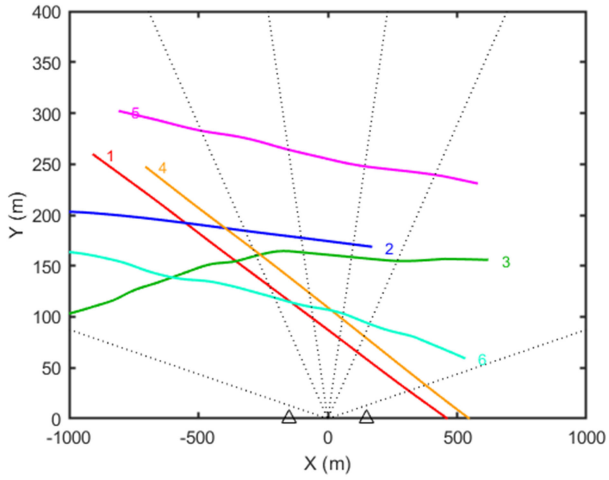

Fig. 7. Locations of ULS compact arrays (symbols "Δ"). The corrected positions of ships used in the test are shown by colored lines. Dotted lines show the boundaries of azimuth sectors for which the average RMSE of the position estimates were computed.

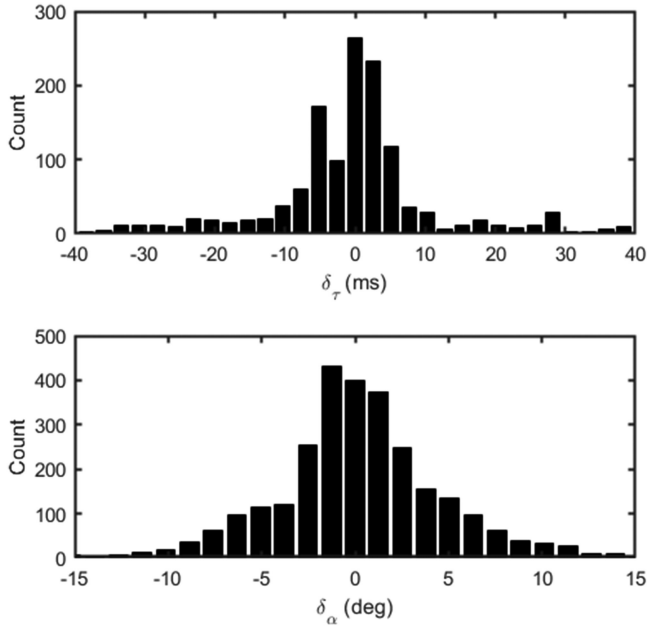

Fig. 8. Histograms of (top) TDOA estimation errors and (bottom) azimuth estimation errors obtained using ULS.

of ships were computed as $\boldsymbol{r_k}(t_p) = \boldsymbol{r}_{k\mathrm{AIS}}(t_p) - \boldsymbol{\delta}_k$, $k = 1,\ldots,K$, $p = 1,\ldots,P$, where $\boldsymbol{r}_{k\mathrm{AIS}}(t_p)$ is the interpolated AIS-based coordinate of the kth ship at time t_p, P is the number of AOA and TDOA measurements of the kth ship, and $\boldsymbol{\delta}_k$ is the estimated offset of the dominant noise source relative to the position of the GPS receiver (see [23] for more details). Ships had lengths from 185 to 337 m; water speeds from 9.9 to 17.7 kn; and their closest points of approach (CPA) to the origin in horizontal plane ranged from 86 to 255 m. The corrected trajectories of ships, $\boldsymbol{r_k}(t)$, are shown in Fig. 7.

Azimuth and TDOA were estimated using ship noise generated within frequency band $f \in [100,\ 1000]$ Hz for nonoverlapping time intervals $T = 0.6$ s long and separated by 1 s. The wideband beamformer presented in [39] was used to estimate azimuths. TDOA was measured for all $M^2 = 16$ pairs of hydrophones as positions of peaks of corresponding cross-correlation functions [39]. For the kth ship, the azimuth error provided by the nth array was computed as $\delta_{\alpha p}^{(n)} = \hat{\alpha}_n(t_p) - \alpha_n(t_p), n = 1,2$, where $\hat{\alpha}_n(t_p)$ is the azimuth estimate obtained by nth array; and $\alpha_n(t_p) = \alpha_n(\boldsymbol{r}_k(t_p))$ is the expected azimuth of the kth ship. TDOA errors were computed as $\delta_{\tau p} = \hat{\tau}(t_p) - \tau(t_p)$, where $\hat{\tau}(t_p)$ and $\tau(t_p) = \tau(\boldsymbol{r}_k(t_p))$ are the estimated and expected values of TDOA, respectively. The STD of AOA and TDOA estimation errors was computed as

$$\hat{\sigma}_{\alpha k}^{(n)} = \sqrt{\mu\left\{\left(\delta_{\alpha 1}^{(n)}\right)^2, \left(\delta_{\alpha 2}^{(n)}\right)^2, \ldots, \left(\delta_{\alpha P}^{(n)}\right)^2\right\}}$$

$$\hat{\sigma}_{\tau k} = \sqrt{\mu\left\{\delta_{\tau 1}^2, \delta_{\tau 2}^{;2}, \ldots, \delta_{\tau P}^2\right\}}, \quad k = 1 \ldots K \qquad (49)$$

where $\mu\{x_1, x_2, \ldots, x_P\}$ is the median value of P random variables $x_1, x_2, \ldots, x_P$.

The total number of TDOA and AOA estimates obtained for $K = 6$ ships was 1483 and 2966, respectively. Histograms of all computed TDOA and azimuth errors are shown in Fig. 8. The average empirical STD of TDOA and AOA estimates computed for all ships was $\hat{\sigma}_\tau = 3.2$ ms and $\hat{\sigma}_\alpha = 2.5°$. A total of 181 TDOA estimates with $|\delta_\tau| > 40$ ms and 212 azimuth estimates with $|\delta_\alpha| > 15°$ were identified as outliers. After excluding outliers, the average empirical STD was $\hat{\sigma}_\tau = 2.5$ ms and $\hat{\sigma}_\alpha = 2.2°$. The STD of AOA estimates obtained for each individual array and each ship used in the tests were $\{[1.0°,\ 1.3°];\ [0.9°,\ 2.4°];\ [3.5°,\ 2.4°];\ [2.1°,\ 3.2°];\ [1.0°,\ 1.8°];[1.4°,\ 1.2°]\}$. The STD of TDOA estimates were $\{2.1; 1.1; 3.2; 1.6; 2.9; 4.1\}$ ms. It was also found that the absolute value of the empirical correlation coefficient between AOA and TDOA measurements was within the range from 0.08 to 0.34 such that AOA and TDOA estimates can be considered as uncorrelated random variables.

The CRB values of the hybrid estimator (43) computed for all ships used in the test as a function of ship azimuths centered at the azimuth of the CPA, $\alpha(t) - \alpha_{\mathrm{CPA}}$, are shown in Fig. 9. This figure demonstrates that for networks with $N = 2$ arrays, position estimation errors strongly depend on the distance and azimuth of the source. Because ship positions changed, computing RMSE for each position $\boldsymbol{r_k}(t_p)$ was not possible. To evaluate relative efficiency, the average empirical RMSE was computed for five azimuth sectors with boundaries of $\{-85°,\ -60°,\ -30°, 30°, 60°, 85°\}$. The average RMSE provided by the AOA-based (symbol "○") and the hybrid (symbol "×") localization algorithms are shown in Fig. 9. Relative empirical efficiency of the AOA and hybrid estimators was $\sigma_A^2/\sigma_H^2 = 1.23 \ldots 1.69$.

VI. Discussions and Conclusion

The results of statistical simulations confirmed that in the case of Gaussian errors, the RMSE of the position estimates provided

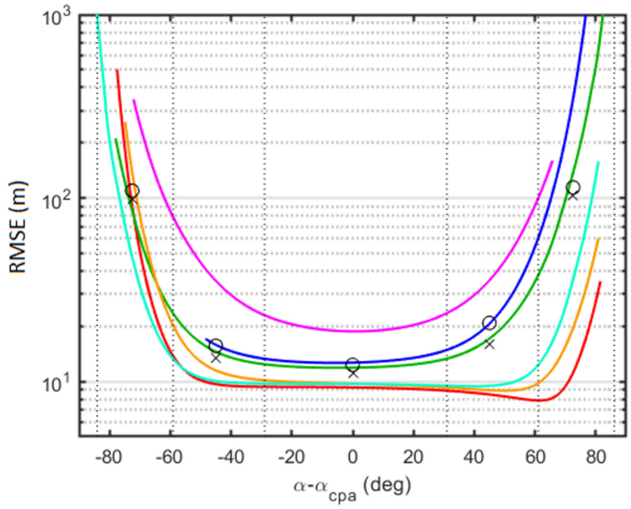

Fig. 9. Average RMSE of positions estimates provided by AOA-based estimator (symbol "○") and hybrid estimator (symbol "×") as a function of ship azimuths. Colored solid lines show the square root of the CRB for the hybrid estimator, $\sqrt{\mathrm{CRB}_{\boldsymbol{h}}}$, computed for each ship. Vertical dotted lines show the boundaries of azimuth sectors for which the average RMSE of the position estimates were computed.

by the ML AOA-based and TDOA-based estimators are well approximated by the CRB. The accuracy of the AOA-based and TDOA-based algorithms strongly depends on the AOA estimation and TDOA estimation accuracy, respectively.

The hybrid ML estimator minimizes the position estimation errors and is more efficient in terms of accuracy than any of AOA-based or TDOA-based estimators. The impact of AOA-based and TDOA-based estimates on the hybrid estimate depends on the number of arrays in the network and on the AOA and TDOA estimation errors. As Fig. 3 shows, for networks consisting of $N \geq 3$ arrays, the RMSE of the hybrid estimates is determined by the TDOA-based estimates, $\sigma_H \approx \sigma_T$, and is almost independent of the AOA estimates if TDOA estimation errors are quite small ($\sigma_\tau \leq 0.1$ ms and $\sigma_\alpha \geq 0.2^\circ$). Similarly, the accuracy of the hybrid algorithm is almost determined by the AOA-based algorithm, $\sigma_H \approx \sigma_A$, and the contribution of the TDOA-based algorithm is negligible if TDOA estimation errors are large ($\sigma_\tau \geq 10$ ms and $\sigma_\alpha \leq 3^\circ$). Simulations showed that both AOA-based and TDOA-based estimators provide comparable impact on the hybrid estimates if $\sigma_\tau \approx 1$ ms and $\sigma_\alpha = 0.2^\circ, \ldots, 3^\circ$. For networks with $N = 2$ arrays, the TDOA-based algorithm cannot be implemented, and both AOA and the hybrid algorithms provide similar accuracy (see Figs. 5 and 9). The practical use of the hybrid estimator in a two-array network may be justified to reduce the likelihood of outliers occurring when condition (32) is violated.

The results of *in situ* test showed that for signals within frequency band $f \in [100, 1000]$ Hz and for the arrays with the half-wavelength frequency of $f_{\lambda/2} \approx 440$ Hz, the empirical STD of TDOA and AOA estimates can be $\hat{\sigma}_\tau \approx 1, \ldots, 4$ ms and $\hat{\sigma}_\alpha \approx 0.9^\circ, \ldots, 3.5^\circ$. These values comply with the previously obtained results presented in [11] and [39].

Empirical data also suggest that large-aperture arrays with omnidirectional sensors ($M = 1$) allowing implementation of the TDOA-based localization algorithms only may provide potentially achievable localization accuracy in the case or small TDOA estimation errors, $\sigma_\tau \leq 1$ ms. But this situation may rarely occur in practice. As test results presented in [11] show, for low-frequency signals, the expected TDOA estimation errors strongly depend on SNR. The empirical error can be $\sigma_\tau \approx 1, \ldots, 50$ ms if SNR $= 10, \ldots, 40$ dB and $\sigma_\tau \approx 50, \ldots, 800$ ms if SNR $= 0, \ldots, 10$ dB. The empirical values of the AOA estimation errors provided by a tetrahedral compact array with $M = 4$ sensors can be $0.2^\circ, \ldots, 3.0^\circ$ for low- and midfrequency impulsive signals with SNR $= 10, \ldots, 35$ dB [39].

Thus, the main conclusion of this work is that networks with synchronized compact arrays can provide significant benefits in terms of using various AOA-based, TDOA-based, and hybrid localization techniques. In general, the hybrid estimator provides higher localization accuracy than any of AOA-based and TDOA-based estimators. But the practical choice of localization technique strongly depends on the AOA and TDOA estimation errors provided by the arrays for a given signal type. For narrowband signals within the frequency range close to the half-wavelength frequency of compact arrays, AOA-based localization techniques can be more accurate than TDOA-based estimators. For high-frequency signals, TDOA-based estimators can be more efficient.

The results from this work make it possible to evaluate the performance of various network configurations before they are deployed. The potential areas of future research include studying the influence of signal parameters on AOA, TDOA, and position estimation accuracy in various real-world scenarios.

ACKNOWLEDGMENT

The authors would like to thank K. Scanlon for editing the draft version of the manuscript. The authors would also like to thank the anonymous reviewers for their comments that helped to improve the quality of this manuscript.

REFERENCES

[1] C. W. Clark and W. T. Ellison, "Calibration and comparison of the acoustic location methods used during the spring migration of the bowhead whale, *balaena mysticetus*, off Pt. Barrow, Alaska, 1984–1993," *J. Acoust. Soc. Amer.*, vol. 107, no. 6, pp. 3509–3517, 2000.

[2] V. Janik, S. Van Parijs, and P. Thompson, "A two-dimensional acoustic localization system for marine mammals," *Mar. Mamm. Sci.*, vol. 16, no. 2, pp. 437–447, 2000.

[3] B. Møhl, M. Wahlberg, and A. Heerfordt, "A large-aperture array of nonlinked receivers for acoustic positioning of biological sound sources," *J. Acoust. Soc. Amer.,* vol. 109, no. 1, pp. 434–437, 2001.

[4] M. H. Laurinolli, A. E. Hay, F. Desharnais, and C. T. Taggart, "Localization of North Atlantic right whale sounds in the Bay of Fundy using a sonobuoy array," *Mar. Mamm. Sci.,* vol. 19, no. 4, pp. 708–723, 2003.

[5] R. Morrissey, S. Jarvis, N. DiMarzio, J. Ward, and D. Moretti, "North Atlantic right whale (Eubalaena glacialis) detection & localization in the Bay of Fundy using widely spaced, bottom mounted sensors," in *Proc. IEEE OCEANS Conf.*, 2006, pp. 1–6.

[6] N. Roy, Y. Simard, and J. Rouat, "Performance of three acoustical methods for localizing whales in the Saguenay – St. Lawrence Marine Park," *Can. Acoust.*, vol. 36, no. 1, pp. 160–164, 2008. [Online]. Available: https://jcaa.caa-aca.ca/index.php/jcaa/article/view/2006

[7] L. Hatch *et al.*, "Characterizing the relative contributions of large vessels to total ocean noise fields: A case study using the Gerry E. Studds Stellwagen

Bank National Marine Sanctuary," *Environ. Manage.*, vol. 42, no. 5, pp. 735–752, 2008.
[8] Y. Simard, N. Roy, and C. Gervaise, "Passive acoustic detection and localization of whales: Effects of shipping noise in Saguenay–St. Lawrence Marine Park," *J. Acoust. Soc. Amer.,* vol. 123, no. 6, pp. 4109–4117, 2008.
[9] P. M. Baggenstoss, "An algorithm for the localization of multiple interfering sperm whales using multi-sensor time difference of arrival," *J. Acoust. Soc. Amer.*, vol. 130, no. 1, pp. 102–112, 2011.
[10] P. M. Baggenstoss, "Processing advances for localization of beaked whales using time difference of arrival," *J. Acoust. Soc. Amer.,* vol. 133, no. 6, pp. 4065–4076, 2013.
[11] I. R. Urazghildiiev and C. W. Clark, "Comparative analysis of localization algorithms with application to passive acoustic monitoring," *J. Acoust. Soc. Amer.*, vol. 134, no. 6, pp. 4418–4426, 2013.
[12] M. Hawkes and A. Nehorai, "Wideband source localization using a distributed acoustic vector-sensor array," *IEEE Trans. Signal Process.*, vol. 51, no. 6, pp. 1479–1491, Jun. 2003.
[13] A. Nehorai and E. Paldi, "Acoustic vector-sensor array processing," *IEEE Trans. Signal Process.*, vol. 42, no. 9, pp. 2481–2491, 1994.
[14] D. Rahamim, J. Tabrikian, and R. Shavit, "Source localization using vector sensor array in a multipath environment," *IEEE Trans. Signal Process.*, vol. 52, no. 11, pp. 3096–3103, Nov. 2004.
[15] K. W. Chung, A. Sutin, A. Sedunov, and M. Bruno, "DEMON acoustic ship signature measurements in an urban harbor," *Adv. Acoust. Vib.*, vol. 2011, 2011, Art no. 952798.
[16] A. Tesei, S. Fioravanti, V. Grandi, P. Guerrini, and A. Maguer, "Localization of small surface vessels through acoustic data fusion of two tetrahedral arrays of hydrophones," in *Proc. Mtgs. Acoust.*, vol. 17, 2012, Art. no. 070050. [Online]. Available: https://doi.org/10.1121/1.4772778
[17] I. R. Urazghildiiev and D. E. Hannay, "Maximum likelihood estimators and Cramér–Rao bound for estimating azimuth and elevation angles using compact arrays," *J. Acoust. Soc. Amer.*, vol. 141, no. 4, pp. 2548–2555, 2017.
[18] S. M. Wiggins, M. A. McDonald, and J. A. Hildebrand, "Beaked whale and dolphin tracking using a multichannel autonomous acoustic recorder," *J. Acoust. Soc. Amer.*, vol. 131, no. 1, pp. 156–163, 2012.
[19] R. Hirotsu *et al.*, "Localization of sperm whales in a group using clicks received at two separated short baseline arrays," *J. Acoust. Soc. Amer.*, vol. 127, no. 1, pp. 133–147, 2010.
[20] S. M. Wiggins, K. E. Frasier, E. E. Henderson, and J. A. Hildebrand, "Tracking dolphin whistles using an autonomous acoustic recorder array," *J. Acoust. Soc. Amer.*, vol. 133, no. 6, pp. 3813–3818, 2013.
[21] M. Gassmann, E. E. Henderson, S. M. Wiggins, M. A. Roch, and J. A. Hildebrand, "Offshore killer whale tracking using multiple hydrophone arrays," *J. Acoust. Soc. Amer.*, vol. 134, no. 5, pp. 3513–3521, 2013.
[22] M. Gassmann, S. M. Wiggins, and J. A. Hildebrand, "Three-dimensional tracking of Cuvier's beaked whales' echolocation sounds using nested hydrophone arrays," *J. Acoust. Soc. Amer.*, vol. 138, no. 4, pp. 2483–2494, 2015.
[23] I. R. Urazghildiiev and D. E. Hannay, "Localizing sources using a network of asynchronous compact arrays," *IEEE J. Ocean. Eng.,* vol. 45, no. 3, pp. 1091–1098, Jul. 2020.
[24] I. R. Urazghildiiev and D. E. Hannay, "Using a stationary compact array of acoustic sensors to estimate the motion parameters of sources," *IEEE J. Ocean. Eng.,* vol. 43, no. 4, pp. 1134–1142, Oct. 2018.
[25] W. M. X. Zimmer, *Passive Acoustic Monitoring of Cetaceans*. Cambridge, U.K.: Cambridge Univ. Press, 2011, p. 366.
[26] W. H. Foy, "Position-location solutions by Taylor-series estimation," *IEEE Trans. Aerosp. Electron. Syst.*, vol. AES-12, no. 2, pp. 187–194, Mar. 1976.
[27] L. Cong and W. Zhuang, "Hybrid TDOA/AOA mobile user location for wideband CDMA cellular systems," *IEEE Trans. Wireless Commun.*, vol. 1, no. 3, pp. 439–447, Jul. 2002.
[28] C. Ma, R. Klukas, and G. Lachapelle, "An enhanced two-step least squared approach for TDOA/AOA wireless location," in *Proc. IEEE Int. Conf. Commun.*, 2003, vol. 2, pp. 987–991.
[29] A. N. Bishop, B. Fidan, K. Doğançay, B. D. Anderson, and P. N. Pathirana, "Exploiting geometry for improved hybrid AOA/TDOA-based localization," *Signal Process.*, vol. 88, no. 7, pp. 1775–1791, 2008.
[30] X. Li, Z. D. Deng, L. T. Rauchenstein, and T. J. Carlson, "Contributed review: Source-localization algorithms and applications using time of arrival and time difference of arrival measurements," *Rev. Sci. Instrum.*, vol. 87, no. 4, 2016, Art. no. 041502.
[31] Y. Wang and K. Ho, "Unified near-field and far-field localization for AOA and hybrid AOA-TDOA positionings," *IEEE Trans. Wireless Commun.*, vol. 17, no. 2, pp. 1242–1254, Feb. 2018.
[32] T. Jia, H. Wang, X. Shen, Z. Jiang, and K. He, "Target localization based on structured total least squares with hybrid TDOA-AOA measurements," *Signal Process.*, vol. 143, pp. 211–221, 2018.
[33] B. Friedlander, "A passive localization algorithm and its accuracy analysis," *IEEE J. Ocean. Eng.,* vol. 12, no. 1, pp. 234–245, Jan. 1987.
[34] K. Yang, G. Wang, and Z.-Q. Luo, "Efficient convex relaxation methods for robust target localization by a sensor network using time differences of arrivals," *IEEE Trans. Signal Process.,* vol. 57, no. 7, pp. 2775–2784, Jul. 2009.
[35] M. Wahlberg, B. Møhl, and P. T. Madsen, "Estimating source position accuracy of a large-aperture hydrophone array for bioacoustics," *J. Acoust. Soc. Amer.,* vol. 109, no. 1, pp. 397–406, 2001.
[36] S. Haykin, *Array Signal Processing*. Englewood Cliffs, NJ, USA: Prentice-Hall, 1985, p. 493.
[37] D. H. Johnson and D. E. Dudgeon, *Array Signal Processing: Concepts and Techniques*. Englewood Cliffs, NJ, USA: Prentice-Hall, 1993, p. 533.
[38] H. L. Van Trees, *Optimum Array Processing: Part IV of Detection, Estimation, and Modulation Theory*. New York, NY, USA: Wiley, 2002.
[39] I. R. Urazghildiiev, B. Martin and D. E. Hannay, "The Accuracy of Bearing Estimates of Wideband Signals Produced by Marine Animals," in *IEEE J. Ocean. Eng.*, early access, 2021, doi: 10.1109/JOE.2020.3040703.
[40] B. F. Cron and C. H. Sherman, "Spatial-correlation functions for various noise models," *J. Acoust. Soc. Amer.,* vol. 34, no. 11, pp. 1732–1736, 1962.
[41] S. M. Kay, *Fundamentals of Statistical Signal Processing*. Englewood Cliffs, NJ, USA: Prentice-Hall/PTR, 1993.
[42] O. Le Bot, Y. Simard, N. Roy, J. I. Mars, and C. Gervaise, "Whistle source levels of free-ranging beluga whales in Saguenay-St. Lawrence Marine Park," *J. Acoust. Soc. Amer.*, vol. 140, no. 1, pp. EL89–EL93, 2016.
[43] A. Širović, J. A. Hildebrand, and S. M. Wiggins, "Blue and fin whale call source levels and propagation range in the Southern Ocean," *J. Acoust. Soc. Amer.,* vol. 122, no. 2, pp. 1208–1215, 2007.
[44] D. Risch, U. Siebert, and S. M. Van Parijs, "Individual calling behaviour and movements of North Atlantic minke whales (*Balaenoptera acutorostrata*)," *Behaviour,* vol. 151, no. 9, pp. 1335–1360, 2014.
[45] S. E. Parks and P. L. Tyack, "Sound production by North Atlantic right whales (*Eubalaena glacialis*) in surface active groups," *J. Acoust. Soc. Amer.,* vol. 117, no. 5, pp. 3297–3306, 2005.

Ildar R. Urazghildiiev received the M.Sc. degree in electrical engineering from Zhitomir Institute of Radioelectronics, Zhitomir, Ukraine, in 1989, and the Ph.D. degree in electrical engineering from the National R&D Center of Defense Technologies and Military Security of Ukraine, Kiev, Ukraine, in 1996.

From 1994 to 2001, he was with the National R&D Center of Defense Technologies and Military Security of Ukraine and the National Technical University of Ukraine "Kiev Polytechnic Institute," Kiev, Ukraine. In 2001 and 2003, he held a Postdoctoral Fellow position at the Signals and Systems Group, Uppsala University, Uppsala, Sweden. From 2004 to 2014, he was a Research Associate with the Lab of Ornithology, Cornell University, Ithaca, NY, USA. In 2014, he joined JASCO Applied Sciences, Inc., Silver Spring, MD, USA, where he is currently a Senior Research Engineer. His research interests include statistical signal processing, signal detection, parameter estimation, classification, localization, and tracking with applications to bioacoustics.

David E. Hannay received the B.Sc. and M.Sc. degrees in physics from the University of Victoria, Victoria, BC, Canada, in 1988 and 1994, respectively.

Since 1989, he has been a research scientist at JASCO Applied Sciences, Victoria, BC, Canada, specializing in underwater acoustic modeling for environmental noise assessments. He is currentlt a Chief Science Officer for JASCO's multinational science teams. He develops computer models for predicting acoustic pressure and particle velocity, and applies those to a variety of industrial noise sources including sonars, explosives, aircraft, seismic exploration sources, shipping, and pile driving. His recent work is related to ship noise measurements and quieting technologies.